Solar Energy Materials & Solar Cells 132 (2015) 282–288

Contents lists available at ScienceDirect

Solar Energy Materials & Solar Cells

journal homepage: www.elsevier.com/locate/solmat

Micro-structural defects in polycrystalline silicon thin-film solar cells on glass by solid-phase crystallisation and laser-induced liquid-phase crystallisation

Jialiang Huang *, Sergey Varlamov, Jonathon Dore, Jae Sung Yun, Martin A. Green

University of New South Wales, Sydney, NSW, Australia

ARTICLE INFO

Article history:
Received 6 June 2014
Received in revised form
9 September 2014
Accepted 15 September 2014

Keywords:
Poly-Si
Thin-film
Solar cell
Laser crystallisation
TEM
Defect

ABSTRACT

The microstructural properties of polycrystalline silicon films obtained by either solid-phase crystallisation (SPC) or laser-induced liquid-phase crystallisation (LPC) were investigated by transmission electron microscopy (TEM). In SPC films, the most common intra-grain defects are dislocations with the density as high as 1E10 cm^{-2} determined from cross-sectional weak-beam dark-field images. The highest dislocation density in LPC film is at least two orders of magnitude lower than the SPC film, 1E8 cm^{-2} and typically it is below 1E6 cm^{-2}. The most common defect type in LPC films is twin boundaries and other junctions of different coincidence site lattice (CSL) boundaries. Such differences in the material structural properties result in far superior electrical performance of solar cells made of LPC films, such as mobility up to 400 $cm^2\,V^{-1}\,s^{-1}$, similar to c-Si wafers, and the higher open-circuit voltage up to 585 mV.

1. Introduction

Thin-film crystalline silicon on glass solar cells have a potential to combine the strengths of c-Si wafer-based photovoltaics with benefits of the thin-film approach. A lot of work has been done to fabricate several microns thick polycrystalline silicon (poly-Si) films using solid phase crystallisation (SPC) and aluminium-induced crystallization (AIC) [1,2]. The record efficiency of 10.4% was demonstrated on a PECVD SPC minimodule on textured borosilicate glass [3]. However, the SPC cell performance was found to be limited by the low open circuit voltage (< 500 mV). It has been confirmed that the low voltage is due to high intra-grain defect density [4–6]. Recently there has been a breakthrough in development of low defect density crystalline silicon thin films on glass by using liquid-phase crystallisation, which led to liquid-phase crystallised silicon on glass (LPCSG) solar cells [7,8]. LPCSG solar cells can be made by either electron-beam or line-focus diode laser crystallisation of 5–15 mm thick ebeam-evaporated silicon films. Laser LPC cells have reached Voc of 585 mV and the highest measured efficiency of 11.7% [2]. More recently, a stabilised efficiency of 11.5% and the highest Voc of 656 mV have been reported for heterojunction silicon thin-film solar cells with an electron-beam LPC absorber [9]. In this work, the defect properties of SPC and LPC Si films are discussed in detail. The intra-grain dislocation density of the two type of the film was determined from cross-sectional weak-beam dark-field TEM images. The twin boundaries and other coincident site lattice (CSL) boundaries in the LPC film were also investigated by cross-sectional TEM.

2. Experiment

SPC and LPC film samples were fabricated from amorphous silicon (a-Si) films deposited either by e-beam evaporation or PEVCD on 3.3 mm thick Schott Borofloat33 glass. The cell doping profile in SPC films was formed by controlled dopant introduction during deposition and it was followed by crystallisation at 600 °C for 20–23 h. The film then received rapid thermal annealing (RTA) at 930 °C for about 2 min. For LPC cells, uniformly doped e-beam evaporated Si films were crystallised by a single scan of a line-focus 808 nm CW diode laser, then the junction was formed by phosphorous diffusion done by either RTA or laser treatment. The structures of both cell types were presented elsewhere [2]. The absorber doping level of all SPC and LPC investigated in this work is about 1E16 cm^{-2}.

TEM specimens were prepared to study the grain quality and the defect density in selected SPC and LPC samples. Fig. 1 shows a representative TEM Weak-Beam-Dark-Field (WBDF) image of a SPC sample. The WBDF TEM imaging was used as an approach to effectively highlight dislocations for determination of their density in the two types of the films. The WBDF technique is an on-axis

* Corresponding author.
E-mail address: jialiang.huang@unsw.edu (J. Huang).

http://dx.doi.org/10.1016/j.solmat.2014.09.021
0927-0248/

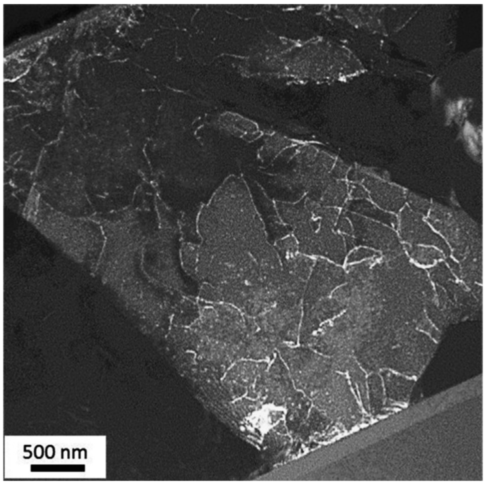

Fig. 1. Representative TEM Weak-Beam-Dark-Field image of SPC sample.

dark field imaging method using a diffraction beam with large excitation error for the defect-free sample area. Thus, the defect free sample area appears dark because of the weak diffraction intensity. However, close to the core of dislocation, the *h k l* plane is bent back into the Bragg condition, which gives rise to a high intensity peak resulting in a very sharp dislocation line near the dislocation core (highly contrasted line in the WBDF image) [10,11]. Then the dislocation density can be estimates from WBDF TEM images by image processing by the following steps: (a) the dislocation lines were drawn and abstracted using image processing software Image-J; (b) the total length of dislocation lines per unit area was calculated at multiple areas; (c) the average dislocation line density per unit area and the standard deviation was calculated for all areas in one image, and (d) the thickness of the TEM foil, which was estimated during sample preparation by FIB, was used to obtain the dislocation line density per unit volume. Besides, defect etching and SEM were used to reveal and investigate the defect structure on the film surface of the LPC samples as well.

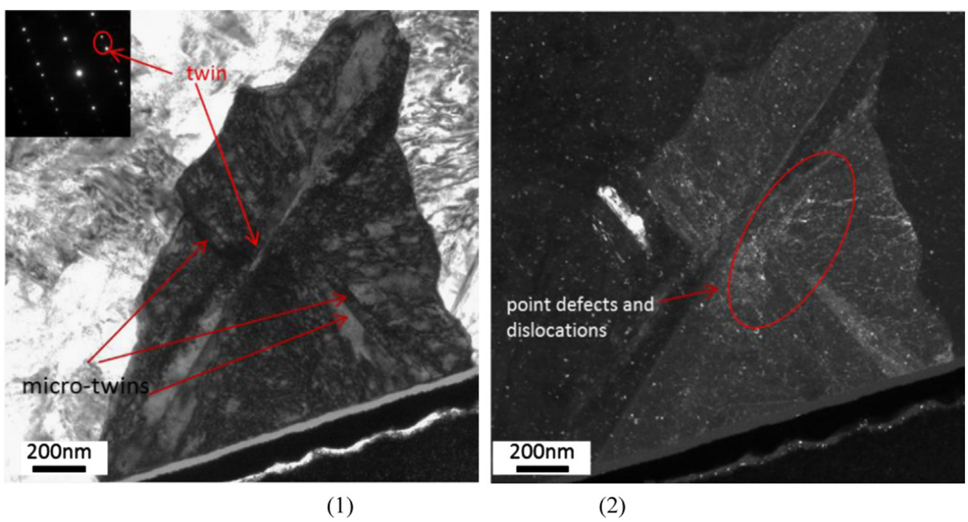

Fig. 2. Bright-field and dark-field TEM images of the sample directly after SPC. (1) Bright-field TEM image and diffraction pattern, (2) diffraction pattern TEM image of the same grain as (1).

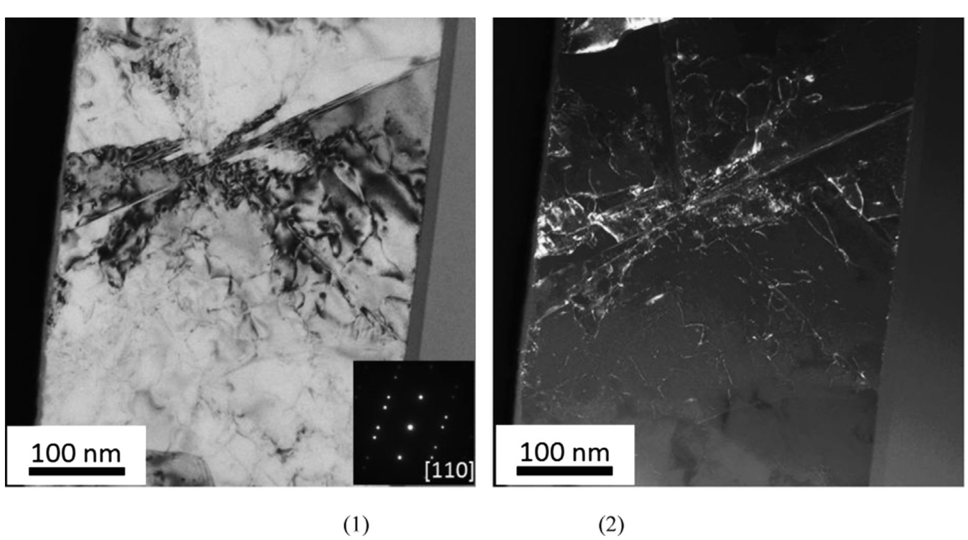

Fig. 3. Bright-field and weak-beam dark-field TEM images of the sample after SPC, (1) bright-field TEM image and diffraction pattern, (2) diffraction pattern TEM image of the same grain as in (1).